INSTITUTE OF PLASMA PHYSICS

NAGOYA UNIVERSITY

RESEARCH REPORT

NAGOYA, JAPAN

Experiments on Ion-Acoustic Solitary Waves*

H. Ikezi

IPPJ-149 JANUARY 1973

Further communication about this report is to be sent to the Reserch Information Center, Institute of Plasma Physics, Nagoya University, Nagoya, JAPAN.

---

* Paper submitted to the Physics of Fluids.

Abstract

Ion-acoustic solitary waves ("Solitons") have been studied experimentally by employing a double-plasma device. The solitary waves are found to be produced from both a single compressional pulse and a continuous wave. A rarefaction pulse also produces solitons if the pulse width is sufficiently wide. A theory based on the Schrödinger equation accounts for the number of solitons. Recurrence to the original state is observed when a continuous wave is launched. A simple wave-wave coupling analysis for the recurrence of the original state is given.

I. INTRODUCTION

A significant number of studies on the nonlinear features of ion-acoustic waves in collisionless plasma have been reported in the last decade. The nonlinear effects in the ion-acoustic waves belong to one of the following two classes depending on the value of the electron-to-ion temperature ratio T_e/T_i. (i) If $T_e/T_i \gtrsim 1$, then the phase velocity of the wave is on the order of the ion thermal velocity and nonlinear wave-particle interactions, such as the trapping of the ions, are the dominant feature of the wave propagation. (ii) If $T_e/T_i \gg 1$, the above mentioned wave-particle interaction is a weak effect, and macroscopic nonlinearities predominate. In this case, the ion temperature may be neglected and the evolution of the one-dimensional small-amplitude, long wavelength ion-acoustic wave can be described by the Kortweg-deVries (K-dV) equation.[1]

$$\frac{\partial \psi}{\partial \xi} + \frac{\partial \psi}{\partial \tau} - \psi \frac{\partial \psi}{\partial \tau} - \frac{1}{2} \frac{\partial^3 \psi}{\partial \tau^3} = 0, \qquad (1)$$

where ψ is the perturbed-to-unperturbed plasma density ratio $\tilde{n}/n_0$ or the wave potential normalized by the electron temperature $e\phi/T_e$, $\xi = x/\lambda_D$ is the spatial coordinate normalized by the electron Debye length λ_D and $\tau = \omega_{pi}t$ is the time normalized by the ion plasma frequency ω_{pi}.

The K-dV equation has been subjected to considerable

theoretical study in recent years. It has been shown that a compressional wave pulse ($\psi > 0$) breaks into a finite number of solitary waves (or "solitons") if it follows the K-dV equation[2-5]. The solution of (1) is also known if $\psi(\tau)$ approaches a constant value sufficiently rapidly as $|\tau| \to \infty$. Numerical analysis of the K-dV equation has shown that a periodic initial value will evolve to form solitons and that the original waveform will be recovered (i.e. "recurrence") after collisions between the solitons[6,7].

We note that the stationary state solution of (1) gives the electron density profile in the solitary wave pulse

$$\tilde{n} = \delta n \, \mathrm{sech}^2[(x - ut)/D] + \tilde{n}_\infty \, , \tag{2}$$

where

$$u = c_s(1 + \tfrac{1}{3} \delta n/n_0) + c_s \, \tilde{n}_\infty/n_0 , \tag{3}$$

and

$$(D/\lambda_D)^2 = 6 \, n_0/\delta n. \tag{4}$$

Here, n_0 is the unperturbed plasma density, δn is the amplitude of the soliton, $\tilde{n}_\infty$ is the value of the perturbation at $x = \infty$, and c_s is the ion-acoustic velocity. From these equations, it follows that as the soliton amplitude increases, its width D decreases and its velocity u increases. It is

also known that only compressional solitons appear in the ion-acoustic branch[8]. Wave-particle interactions due to finite ion temperature would modify the relations (2) and (3) and would cause damping of the solitons[9].

In a previous note[10], the experimental observation of the formation and the interaction of the ion-acoustic solitons have been reported. The present paper is an extension of the previous work to describe other properties of the ion-acoustic solitons. The experimental conditions and methods are described in Section II. The experimental results which are described in Section III include: (A) The relations between the amplitude, the width and the velocity of the solitons and other basic properties; (B) The dependence of the number of solitions on the initial boundary values; and (C) the observation of the recurrence phenomenon. A discussion of each topic described in Section III is presented in Section IV. The conclusions of the present study are summarized in Section V.

II. EXPERIMENTAL CONDITIONS AND METHODS

The experiment is carried out in a double-plasma (DP) device[11]. The apparatus consists of two identical but electrically independent conducting vacuum chambers, made of 50 cm diameter cylinders, each of 40 cm length. A fine mesh grid (40 wires/cm) partitions the space into two regions. Typical

plasma parameters are; plasma density $n_0 = 10^9 \sim 10^{10} cm^{-3}$; electron temperature $T_e \simeq 3$ eV; ion temperature $T_i < 0.2$ eV; argon gas pressure $P = (1 \sim 3) \times 10^{-4}$ Torr. The application of voltage signals to one chamber relative to the other chamber efficiently launch density perturbations through the grid[11,12]. The electron density perturbations are observed by monitoring the electron saturation current of Langmuir probe. The ion distribution is monitored by an electrostatic energy analyzer.[13]

To characterize the ion-acoustic wave behavior in this plasma, we present an experimentally measured dispersion curve for small amplitude waves ($\tilde{n}/n_0 \sim 10^{-3}$) in Fig.1. The solid curve A shows the dispersion relation obtained by linearizing (1) and curve B shows that calculated from the dielectric function[14]

$$\varepsilon = 1 + \frac{k_D^2}{k^2} \left[1 - \frac{T_e}{2T_i} Z'\left(\frac{\omega}{kv_i}\right)\right] = 0 \qquad (5)$$

for $T_e/T_i = 30$. The approximation, to the order $(\omega/\omega_{pi})^3$, involved in (1) is satisfactory in the range $\omega/\omega_{pi} < 0.7$ where our experiments have been performed.

III. EXPERIMENTAL RESULTS

The formation of the solitons is exhibited in Fig.2, (and has been reported earlier[10]). Relatively large-amplitude compressional wave, excited by the applied potential pulse

shown in the top trace, steepens and develops an oscillatory structure. Finally the initial single humped wave is divided into a train of many peaks. The precursor is a group of streaming ions reflected from the wave front as observed with the energy analyzer. If the original wave amplitude are decreased, then a longer distance is required for steepening to occur and a fewer number of peaks are produced. The small-amplitude wave ($\tilde{n}/n_0$ is a few percent) simply damps before steepening. The damping is mainly due to Landau damping. We now describe, in detail, further experimental findings.

A. Basic Properties

Large amplitude wave pulses are obtained when the width or the amplitude of the original wave is increased. The effect of changing the pulse amplitude on the width and the propagation velocity is measured. This result is shown in Fig.3. As the amplitude of the compressive pulse is increased (decreased), the width decreases (increases) and the velocity increases (decreases). Note that the velocity is faster than c_s, i.e., the Mach number is greater than unity. Here, c_s is obtained experimentally from measurements of a very small-amplitude ion-acoustic wave. These features of the pulses identify them as solitons. The experimental points systematically deviate[9,15] from the lines given by equations (3) and (4), where we have set $n_\infty = 0$.

Apparently finite ion-temperature effects such as ion reflection cause damping of the solitons. The bars in Fig.3 show the ranges of the amplitude where the averaged propagation velocity has been measured.

It should be noted that the formation of the soliton is sensitive to the value of T_e/T_i and also to contamination by light ions.[16] When T_e/T_i is low, say 10, or the light ions are present, say hydrogen "out gassed" from the chamber wall, the wave does not break into solitons but induces turbulent noise[17,18]. The amplitude of the solitons $\delta n/n_0$ in these experiments is smaller than 0.2. The amplitude of the precursor increased sharply when the amplitude of the solitons is increased and a heavier damping results.

It is observed that a rarefaction wave pulse also produces solitons when its width is wider than the width of the soliton. As the rarefaction wave propagates, the rising part of its density steepens and a train of peaks follow. The velocity of the solitons is slower than c_s which is presumably due to the fact that $\tilde{n}_\infty < 0$ in (2) and (3). No rarefaction soliton is found. Although the wave train is generated when the width of the original pulse is narrower than that of the solitons, it is hard to identify each peak as a soliton using our previously described criteria. The period of the oscillations[19] in the time domain is observed to increase proportionally with $x^{1/3}$

and with $\phi_{ex}^{-1/2}$. Here, ϕ_{ex} is the amplitude of the potential applied to the wave exciter.

B. Number of Solitons

The number of solitons is increased when the amplitude or the width of the exciting pulse is increased[20]. Representative pictures, showing the relation between the wave excitation pulses and the received electron density perturbation signals picked up at x = 8 cm with the pulse width as a parameter, are shown in Fig.4. The two traces at the top show five solitons when the total width of the excitation pulse is 5 μs. Narrower excitation pulses generate a fewer number of solitons as shown in the following traces. Although the amplitude of the excitation pulse is kept constant, the resulting amplitude of the largest soliton in each case is smaller when the width of the excitation pulse is narrower. It should be noted that the wave train, which is at later times of the picture, follows behind two solitons in the bottom trace.[3] The dependence of the number of solitons on the amplitude is observed to be weak, although the range of the amplitude studied experimentally is narrow because the small-amplitude wave damps before making solitons and larger values of excitation voltage inject an ion-beam into the plasma[20,21].

The shape of the excitation pulses in Fig.4 is one cycle

of a sinusoidal wave. It is found that the waveform after breaking into the solitons is almost independent of the original shape of this pulse provided that the pulse width was the same in the sense as described in the next section [see Fig.4(b)].

C. Periodic Wave and Recurrence of the Initial Waveform

Continuous sinusoidal waves are also found to generate solitons. Figure 5 shows the spatial evolution of a wave excited by sinusoidal signals. These plots, in which the abscissa is axial position, are obtained by sampling the saturated electron current from a Langmuir probe at a fixed phase of the excitation signal while sweeping the probe position. The sinusoidal wave steepens and generates the solitons in one fundamental cycle (see third or fourth cycle on the top trace) when the frequency of the excitation signal $\omega_0/2\pi$ is low. The number of solitons generated in each fundamental period of the original waveform is the same as that found in the experiment where a single-humped perturbation is launched, provided that the width and the amplitude of the pulse are the same as those of the sinusoidal wave. Since the small soliton is delayed from the larger ones, the fourth smallest soliton is absorbed into the largest soliton at the fifth cycle from the left in the case for $\omega_0/2\pi = 0.15$ MHz shown on the top trace. (The width of the soliton is

wider at a larger distance. However, this is not real but is due to jittering of the wave velocity induced by a ripple from the power supply. The sampling method averages the signal.) A different kind of interaction is seen at the end of the third trace where $\omega_0/2\pi$ = 0.25 MHz. Two peaks do not merge into a single peak[10]. It is observed that two solitons fused and formed a single peak when one of them is very small compared with the other one. If the amplitudes of the interacting solitons are comparable, then the two peaks do not form a single peak during the interaction. In the case of the trace at the bottom, a small peak is at the bottom of the wave trough in the early few cycles. This peak is not the signal due to the reflected ions because its velocity is slower than that of the large peak. It is found that the waveform is sinusoidal at the middle of the trace.

The recurrence of the waveform to the original sinusoidal signal is illustrated in Fig.6(a) more clearly. The sinusoidal wave steepens as it propagates and forms two solitons at x = 5 cm. The original sinusoidal waves is recovered[22] at x = 9 cm, and again the signal starts steepening. (Broadening of the trace line is due to a jitter in the wave velocity as noted above.) The Fourier amplitudes of the fundamental frequency and of the higher harmonics are plotted in Fig.6(b) as a function of distance. The fundamental wave damps and the second harmonic grows originally. After x = 5 cm,

however, the fundamental wave grows and the second harmonic damps and completely disappears at x = 9 cm where recurrence of the wave is observed. The amplitude of the third harmonic is not large. It is observed that a larger-amplitude wave shortens the recurrence distance and shows less perfect recurrence.

A typical result from interferometer measurement is shown in Fig.7, in the case when the nonlinearity of the wave is comparable with the dispersion. The measurement of the second harmonic wave is carried out by feeding a signal with frequency equal to $2\omega_0$ to the interferometer as a reference signal. The phase of this reference signal is locked to the wave excitation signal ω_0. Only the $2\omega_0$ component of the wave signal detected by the probe is selected by using a filter. The amplitude of the fundamental wave is almost spatially constant in this case. The second harmonic wave initially grows and then damps. The recurrence is seen at x = 8 cm. A careful comparison of the phase of the two interferometer signals shows that the second harmonic wave propagates with a slower velocity than that of the first harmonic wave, this explains the delay of the small peak. Indeed, a linear superposition of the two signals corresponds to the trace at the bottom of Fig.5. The lower trace in Fig.7 shows a phase jump at x = 8 cm. This fact suggests that the wave at $2\omega_0$ consists of two waves which have slightly different

wavenumbers.

Similar measurements have been performed for the case when ω_0 is smaller and more solitons are found to be generated in a fundamental cycle. The results are as follows: (i) It is found that the harmonics from the first to the N-th are the principal modes in the case when N solitons are generated. The amplitude of the harmonics higher than N-th harmonic is small. In other words, the superposition of the harmonics up to N-th basically describe the waveform. (ii) The periodic spatial amplitude oscillations, like the one shown in Fig.7, are found for every harmonic except for the fundamental. The period of the oscillations is shorter for the larger harmonic number. This fact suggests that the original waveform reappears at the place where the nodes of all principal harmonics coincide[23]. (iii) The propagation velocity of the higher harmonic waves is faster than that of a small-amplitude wave which is excited at the same frequency by an external source and which would be on the linear dispersion curve. However, they were slower than that of the fundamental wave. This fact is related to the feature that a smaller-amplitude soliton is slower than a larger-amplitude soliton. (iv) The distance which is necessary for recurrence of the original waveform increases very critically when ω_0 is decreased.

IV. DISCUSSIONS

A. Basic Properties

The observed dependence of the velocity and the width on the amplitude of the solitary wave pulses is consistent with that described by Eqs.(3) and (4). The systematic deviation of the observed velocity and the width from the predictions of (3) and (4) may be due to finite ion temperature effects[9] or due to the fact that the electrons do not exactly obey the Boltzmann distribution.[10]

Concerning the damping of the solitons, we note the invalidity of invoking a linear Landau damping explanation in the present experiment. Since the soliton has a finite positive potential amplitude ϕ_0, ions in the velocity range $u - (2e\phi_0/M)^{1/2} < v < u$ are reflected by the soliton and carry away the wave energy and damp the soliton. Here, $u \simeq c_s$. The width of the velocity range where the ions are reflected is written as

$$\left(\frac{2e\phi_0}{M} \right)^{1/2} = \left(\frac{\delta n}{n_0} \right)^{1/2} \left(\frac{T_e}{T_i} \right)^{1/2} v_i, \qquad (6)$$

where v_i is the ion thermal velocity and we have used the fact $\delta n/n_0 = e\phi_0/T_e$. If we use typical experimental numbers $\delta n/n_0 = 0.1$ and $T_e/T_i = 30$, then we have $(2e\phi_0/M)^{1/2}/v_i = 1.7$. The analysis of linear Landau dmaping, which assumes that this ratio is very small, apparently is not applicable.

Note that the velocity $u - (2e\phi_0/M)^{1/2}$ is only twice as large as v_i and a significant number of ions are thought to be reflected although the ion distribution function is very small at $v = u(\simeq 4v_i)$. In fact, the assumption, that all of the ions in the range $u - (2e\phi_0/M)^{1/2} < v < u$ are reflected, accounts for the observed amplitude of the precursor. The damping due to this reflection of the ions seriously limits the amplitude of the soliton.

B. Number of Solitons

We compare the observed number of solitons due to the wave excited at $x = 0$ with the theory of Gardner et al.[2] According to their theory, the number of solitons equals the number of the bound states of the following Schrödinger equation;

$$\frac{\partial^2 f(\tau)}{\partial \tau^2} + \frac{1}{3}[\psi(\tau, 0) - \mu] f(\tau) = 0, \qquad (7)$$

provided the K-dV equation [Eq.(1)] describes the evolution of the wave. Here, μ is the eigenvalue which is to be determined, and $\psi(\tau, 0)[= \tilde{n}(\omega_{pi}t, x = 0)/n_0]$ is the density perturbation at $x = 0$ where the wave is launched. Except for the case shown in Fig.5(b), the boundary values in our experiments can be described by

$$\psi(\tau, 0) = \begin{cases} \frac{\psi_0}{2}[1 + \cos(\frac{\pi\tau}{\Delta})], & \text{for } -1 \leq \frac{\tau}{\Delta} \leq 2p + 1 \\ 0 \quad , & \text{elsewhere} \end{cases} \tag{8}$$

where p is zero or a positive integer and $\psi_0 > 0$.

If we introduce the following variables and parameters

$$z = \frac{\pi}{2\Delta}\tau, \qquad a = \frac{1}{3}(\frac{2\Delta}{\pi})^2(\frac{\psi_0}{2} - \mu), \tag{9}$$

$$\text{and} \qquad q = \frac{1}{3\pi^2}\psi_0\Delta^2,$$

then Eq.(7) can be written in the form of a Mathieu equation

$$\frac{d^2f}{dz^2} + [a - 2q\cos(2z)]f = 0. \tag{10}$$

Here, $q = 0$ and $a = a_0 \equiv -3^{-1}(2\Delta/\pi)^2\mu$ for $z \leq 0$ and $z \geq \pi(p+1)$. The solution of (10) has a form[24]

$$f = f_{II} = A\exp(i\nu z)R(z) + B\exp(-i\nu z)R(-z), \tag{11}$$

in the region $0 \leq z \leq \pi(p+1)$,

$$f = f_I = C\exp[(-a_0)^{1/2}z] \qquad \text{for } z \leq 0, \tag{12}$$

and

$$f = f_{III} = D \exp[-(-a_0)^{1/2} z] \qquad \text{for } z \geq \pi(p+1). \quad (13)$$

Here, R(z) is a periodic function with period π. The conditions for a smooth connection of these functions at z=0 and $z = \pi(p+1)$ are;

$$\frac{df_{II}}{dz} / f_{II}\Big|_{z=0} = (-a_0)^{1/2} \text{ and } \frac{df_{II}}{dz} / f_{II}\Big|_{z=\pi(p+1)} = -(-a_0)^{1/2}. \quad (14)$$

For the bound state, $\mu > 0$; therefore $(-a_0)^{1/2}$ is a real number. The boundary conditions (14) lead to the conclusion that one eigen state is determined when the characteristic exponent ν changes from $\ell/(p+1)$ to $(\ell+1)/(p+1)$, where ℓ is zero or a positive integer. There exist p+1 eigen states in each range $0 \leq \nu \leq 1$, $1 \leq \nu \leq 2$, ·····. The eigenvalues a of Eq.(10) are plotted in Fig.8 as a function of q with ν as a parameter[24]. When ν changes from 0 to 1, the curve $a = a(q)$ moves from the curve α_1 to β_1 which are specified in the figure. When ν changes from 1 to 2, $a = a(q)$ moves from α_2 to β_2 and so on. No eigenvalue exists in the regions between the curves β_1 and α_2, β_2 and α_3, ·····. The bound states; $\mu > 0$, exist only in a region specified by $a < 2q$.

Let us consider the simplest case; p=0, which states

that one compressional pulse is excited at the boundary. If we specify the width Δ and the amplitude ψ_0, then q is determined. Since one eigen state exists in each region $0 < \nu < 1$, $1 < \nu < 2$, ·····, therefore only one soliton is generated when $q_1 > q > 0$, two solitons are generated when $q_2 > q > q_1$, and so on ·····. The values of q_1, q_2, ····· are shown in Fig.8. The number of solitons N predicted by the above analysis is indicated by bars in Fig.9 as a function of $\psi_0^{1/2}\Delta$. The experimental data points show that N is linearly proportional to $\psi_0^{1/2}\Delta$ but a systematic deviation from the calculated values is observed. This deviation may be related to that found in Fig.3(a). Since the width of the soliton is narrower than the prediction of Eq.(4), more solitons would be generated than the number predicted by above calculation.

We note, here, the following point: Since Eq.(6) is unchanged under the transformation; $\gamma\tau \rightarrow \tau$ and $\psi(\tau, 0) \rightarrow \gamma^2\psi(\tau, 0)$ where γ is an arbitrary constant number, the number of solitons is unchanged when the waveform $\psi(\tau, 0)$ is varied if the quantity $\int \psi^{1/2}(\tau, 0)d\tau$ is kept constant. This prediction is experimentally confirmed in Fig.4(b). The theory of Gardner et al.[2] also predicts that the amplitude of the soliton should be proportional to the eigenvalue μ. The eigenvalues using the estimate given above account for the observed amplitude ratios between the solitons generated

from the original compressional pulse.

We now discuss the behaviour of the solitary wave excited by a continuous sinusoidal wave. If $\psi(\tau, 0)$ oscillates continuously from $-\infty$ to ∞, then the analysis based on Eq.(7) does not apply. However, if we let p be a large but finite number, we can simulate the experimental condition. In order to describe the situation, we select q, for example in the range $\mathbf{r}_4 < q < q_4$ in Fig.8. The curves α_1 and β_1 touch each other at the value of q that we have specified, such that the p+1 eigenstates degenerate. If we imagine the situation that each cycle of the original wave is separated from the other cycles, i.e., we have p+1 separate pulses, then each pulse has a bound state whose eigenvalue is given by the curve α_1 (or β_1). Therefore each pulse generates one soliton. Since these p+1 eigenstates are still degenerate even after the pulses are pushed together and form a continuous wave, each cycle steepens and produces one soliton which has an amplitude determined by the curves α_1 and β_1. The situation is the same for curves α_2 and β_2, α_3 and β_3. The curves α_4 and β_4 clearly separate from each other. Since the eigenvalues are distributed uniformely between these two curves, the amplitudes of the solitons generated from the different wave periods are not equal. As long as $\mathbf{r}_4 < q < q_4$, four solitons are produced before their interactions. However, when $q_3 < q < \mathbf{r}_4$, three

or four solitons are produced in a wave period. This is due to the fact that p is a finite number so that our boundary value does not have a perfectly monochromatic frequency spectrum.

The above analysis accounts for the experimentally observed result, "The number of solitons generated in each wave period is the same as that of solitons generated from a single humped pulse with the same amplitude and the width", if we ignore the uncertainty appearing in the above analysis.

C. Recurrence of the Sinusoidal Wave

We consider here, the simplest case shown in Fig.7 where the nonlinearity is not stronger than the effect due to wave dispersion and only the fundamental and the second harmonics are the dominant waves. We calculate the period of the amplitude oscillation of the second harmonic wave which gives us the recurrence distance. Since the amplitudes of the harmonics higher than the third one are observed to be small, the first harmonic will be the main driving source in generating the second harmonic. We assume that the first harmonic can be written as

$$\psi_1(\tau,\xi) = \psi_0 \exp[i(k_0\xi - \Omega_0\tau)] \qquad (15)$$

in normalized quantities. Here, K_0 and Ω_0 satisfy the linear dispersion relation

$$K = \Omega + \frac{1}{2}\Omega^3. \tag{16}$$

Employing Eq.(1), the second harmonic $\psi_2(\xi)\exp(-i2\Omega_0\tau)$ follows

$$\frac{\partial\psi_2(\xi)}{\partial\xi} - iK_0\psi_2 + i\Omega_0\psi_0{}^2\exp(i2K_0\xi) = 0, \tag{17}$$

where

$$K_2 = 2\Omega_0 + \frac{1}{2}(2\Omega_0)^3. \tag{18}$$

We impose the boundary condition $\psi_2(0) = 0$ since only the fundamental wave is excited at $\xi = 0$. Then the solution of (17) is

$$\psi_2 = \frac{\psi_0{}^2}{3\Omega_0{}^2}\,[\exp(i2K_0\xi) - \exp(iK_2\xi)]. \tag{19}$$

ψ_2 consists of two waves, as we have measured in Fig.7. One of them has the wavenumber $2K_0$ and is the forced oscillation of the fundamental wave. The other is the one that follows the dispersion relation of the ion-acoustic wave (16). These two waves "beat" and $\psi_2 = 0$ at the diatances given by

$$\xi_R = \ell \frac{2\pi}{3\Omega_0^3} \quad , \tag{20}$$

where ℓ is a positive integer. The same result has been obtained by Tappert and Judice[7]. If ω_0 is much smaller than ω_{pi}, then the recurrence distance X_R is given approximately by

$$\frac{X_R}{\lambda_0} = \frac{1}{3} \left(\frac{\omega_{pi}}{\omega_0}\right)^2 \quad , \tag{21}$$

where λ_0 is the wavelength of the fundamental wave. In the case of Fig.7, $\omega_{pi}/\omega_0 = 5.5$ so that (21) predicts $X_R/\lambda_0 = 10$, while it is 12 experimentally. The above analysis assumes that the third term in Eq.(1) is smaller than fourth term. However, its result agrees with the experimental result performed under the conditions that the above two terms are comparable with each other.

V. CONCLUSIONS

The following results on solitary waves or solitons have been obtained: (i) The compressional ion-acoustic pulses which satisfy the relation between the amplitude, the Mach number and the width of the solitary wave are observed. A systematic deviation of the data points from Eqs.(3) and (4) is found. (ii) The maximum amplitude of the soliton generated in the present experimental scheme is

$\delta n/n_0 \simeq 0.2$. (iii) The number of solitons produced from both a single compressional pulse and a continuous sinusoidal wave is measured and is explained reasonably well using the theory of Gardner et al. (iv) The number and the amplitude of the solitons are found to be insensitive to the original waveform. (v) The recurrence of the original sinusoidal wave is observed and analyzed under conditions of a weak nonlinearity. (vi) The wave does not break into solitons when T_e/T_i is not large nor when light ions are present. (vii) A precursor is found in front of the solitons and its amplitude is large when the amplitude of the soliton is large. The precursor consists mainly of the ions that are reflected by the potential of the soliton and this induces an enhanced damping of the solitons.

ACKNOWLEDGMENT

The author thanks helpful discussions with professor T. Taniuti, Dr. R. J. Taylor, Dr. D. R. Baker, and Dr. K. E. Lonngren.

References

1. H. Washimi and T. Taniuti, Phys. Rev. Lett. 17, 996 (1966). M. Kono and H. Sanuki, J. Phys. Soc. Japan 33, 1731 (1972). Eqs.(1) is written in the laboratory frame. The alternative expression is $(\partial\psi/\partial\tau)+(\partial\psi/\partial\xi)+\psi(\partial\psi/\partial\xi) + \frac{1}{2}(\partial^3\psi/\partial\xi^3) = 0$.

2. C. S. Gardner, J. M. Green, M. D. Kruskal and R. M. Miura, Phys. Rev. Lett. 19, 1095 (1967).

3. N. J. Zabusky, Phys. Rev. 198, 124 (1968).

4. V. I. Karpman, Phys. Lett. 25A, 708 (1967).

5. R. Hirota, Phys. Rev. Lett. 27, 1192 (1971).

6. N. J. Zabsky and M. D. Kruskal, Phys. Rev. Lett. 15, 240 (1965).

7. F. D. Tappert and C. N. Judice, Phys. Rev. Lett. 29, 1308 (1972).

8. R. Z. Sagdeev, Reviews of Plasma Physics (Consultant Bureau, New York, 1969) Vol.IV.

9. P. H. Sakanaka, Phys. Fluids 15, 304 (1972).

10. H. Ikezi, R. J. Taylor and D. R. Baker, Phys. Rev. Lett. 25, 11 (1970).

11. R. J. Taylor, K. R. MacKenzie and H. Ikezi, Rev. Sci. Instr. 43, 1675 (1972).

12. R. J. Taylor, D. R. Baker and H. Ikezi, Phys. Rev. Lett. 24, 206 (1970). H. Ikezi, Y. Kiwamoto, K. Nishikawa and K. Mima, Phys. Fluids 15, 1605 (1972).

13. H. Ikezi and R. J. Taylor, J. Appl. Phys. 41, 738 (1970).

14. B. D. Fried and R. W. Gould, Phys. Fluids 4, 139 (1960).

15. The experimental values of $(D/\lambda_D)^2$ shown in Ref.9 are in fact twice as large as stated there. The authors made a numerical mistake during the course of the analysis of the experimental data.

16. I. Alexeff, W. D. Jones and D. Montgomery, Phys. Rev. Lett. 19, 422 (1967).

17. A. Y. Wong and R. W. Means, Phys. Rev. Lett. 27, 973 (1971).

18. R. A. Stern and J. F. Decker, Phys. Rev. Lett. 27, 1266 (1971).

19. Yu. A. Berezin and V. I. Karpman, Zh. Eksp. Teor. Fiz. 51, 1557 (1966). [Soviet Phys. JETP 24, 1049 (1967)].

20. N. Hershkowitz, T. Romesser and D. Montgomery, Phys. Rev. Lett. 29, 1586 (1972).

21. R. J. Taylor and F. V. Coroniti, Phys. Rev. Lett. 29, 34 (1972).

22. R. Hirota and K. Suzuki, J. Phys. Soc. Japan 28, 1366 (1970).

23. E. Fermi, J. Pasta and S. Ulam, in Enrico Fermi Collected Papers (Univ. of Chicago Press, Chicago, 1965) Vol.II, pp. 977-988.

24. M. Abramowitz and I. A. Stegun, Handbook of Mathematical Functions (Dover Publications, Inc., New York, 1968).

Figure Captions

Fig.1. Dispersion relation of small-amplitude ion-acoustic waves. Dots are experimental points; curves A and B show $k/k_D = (\omega/\omega_{pi})[1 + \frac{1}{2}(\omega/\omega_{pi})^2]$ [see Eq.(1)] and Eq.(5), respectively.

Fig.2. Plot of the electron density perturbation(electron saturation current to the probe)versus time with distance from the wave excitation points, x, as a parameter.

Fig.3. The width D and the velocity u of the solitary waves as a function of its amplitude δn. The solid lines show Eqs.(3) and(4) for $\tilde{n}_\infty = 0$.

Fig.4. Excitation potential pulses, labeled by A_i (1V/div.) and perturbed electron density $\tilde{n}$, labeled by B_i. (a) Wave responses to the sinusoidal pulses. x = 8 cm $\omega_{pi}/2\pi$ = 2.0 MHz. (b) Wave responses to three different shape pulses. x = 11 cm.

Fig.5. Spatial plot of the wave propagation excited by the continuous sinusoidal wave at various frequencies. The time is fixed. $\omega_{pi}/2\pi$ = 2.6 MHz.

Fig.6. (a) Wave response to the sinusoidal wave excitation. The sinusoidal wave is recovered at x = 9 cm.
(b) Spatial amplitude variation of each harmonics.
$\omega_0/2\pi$ = 0.35 MHz. $\omega_{pi}/2\pi$ = 2.0 MHz.

Fig.7. Interferometer output for fundamental wave, A, and second harmoic, B, as a function of distance.
$\omega_0/2\pi$ = 0.4 MHz. $\omega_{pi}/2\pi$ = 2.2 MHz.

Fig.8. A diagram showing the behaviour of the eigenvalue of Eq.(10).

Fig.9. Number of solitons as a function of $\psi_0^{1/2}\Delta$ when the boundary value is $\psi = (\psi_0/2)[1 + \cos(\pi\tau/\Delta)]$ for $|\tau/\Delta| \leq 1$ and $\psi = 0$ elsewhere. $\psi = \tilde{n}/n_0$ and $\tau = \omega_{pi}t$. Bars show theoretical numbers calculated from Eq.(7) and dots are experimental points.

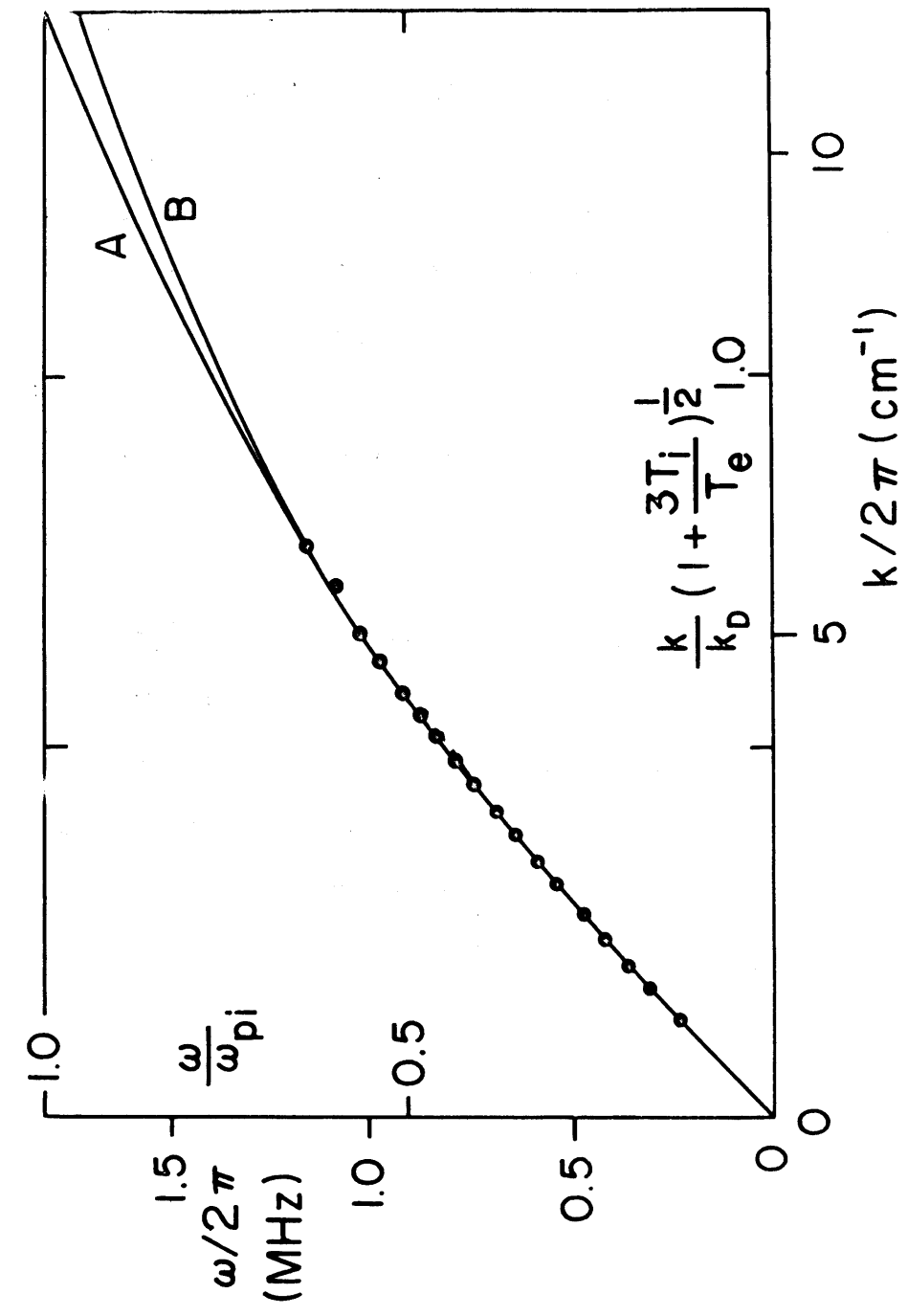
A
B
1.0
0.5
0
$\frac{\omega}{\omega_{pi}}$
1.5
1.0
0.5
0
$\omega/2\pi$ (MHz)
0
5
10
$\frac{k}{k_D}\left(1+\frac{3T_i}{T_e}\right)^{\frac{1}{2}}$
1.0
$k/2\pi$ (cm^{-1})

FIG. 1

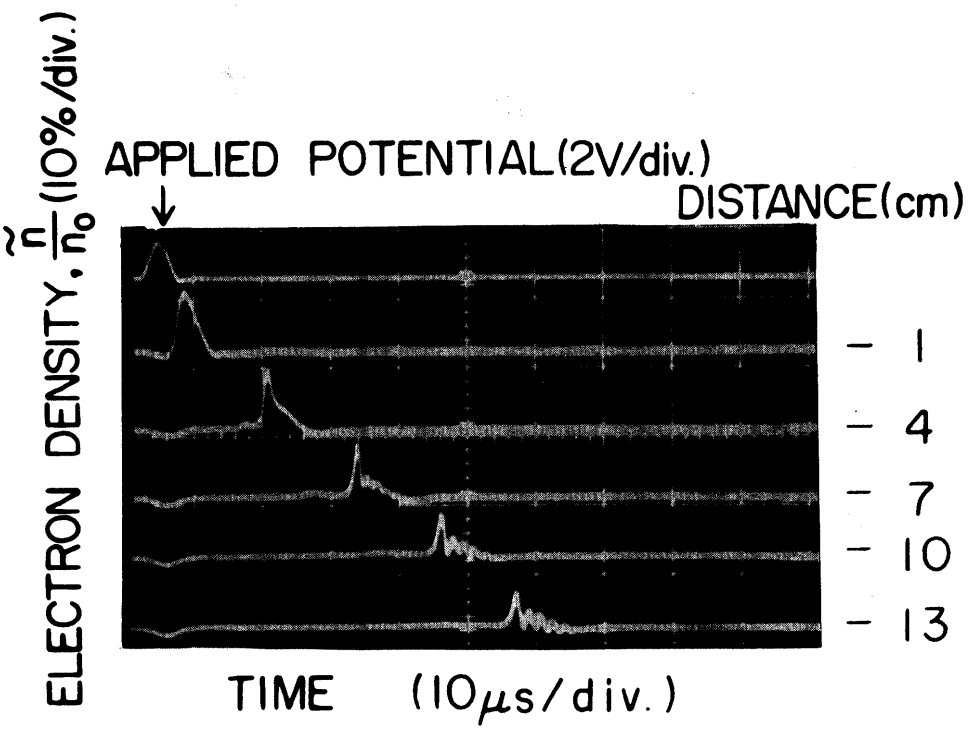
ELECTRON DENSITY, $\frac{\tilde{n}}{n_0}$ (10%/div.)
APPLIED POTENTIAL(2V/div.)
DISTANCE(cm)
1
4
7
10
13
TIME (10μs/div.)

FIG. 2

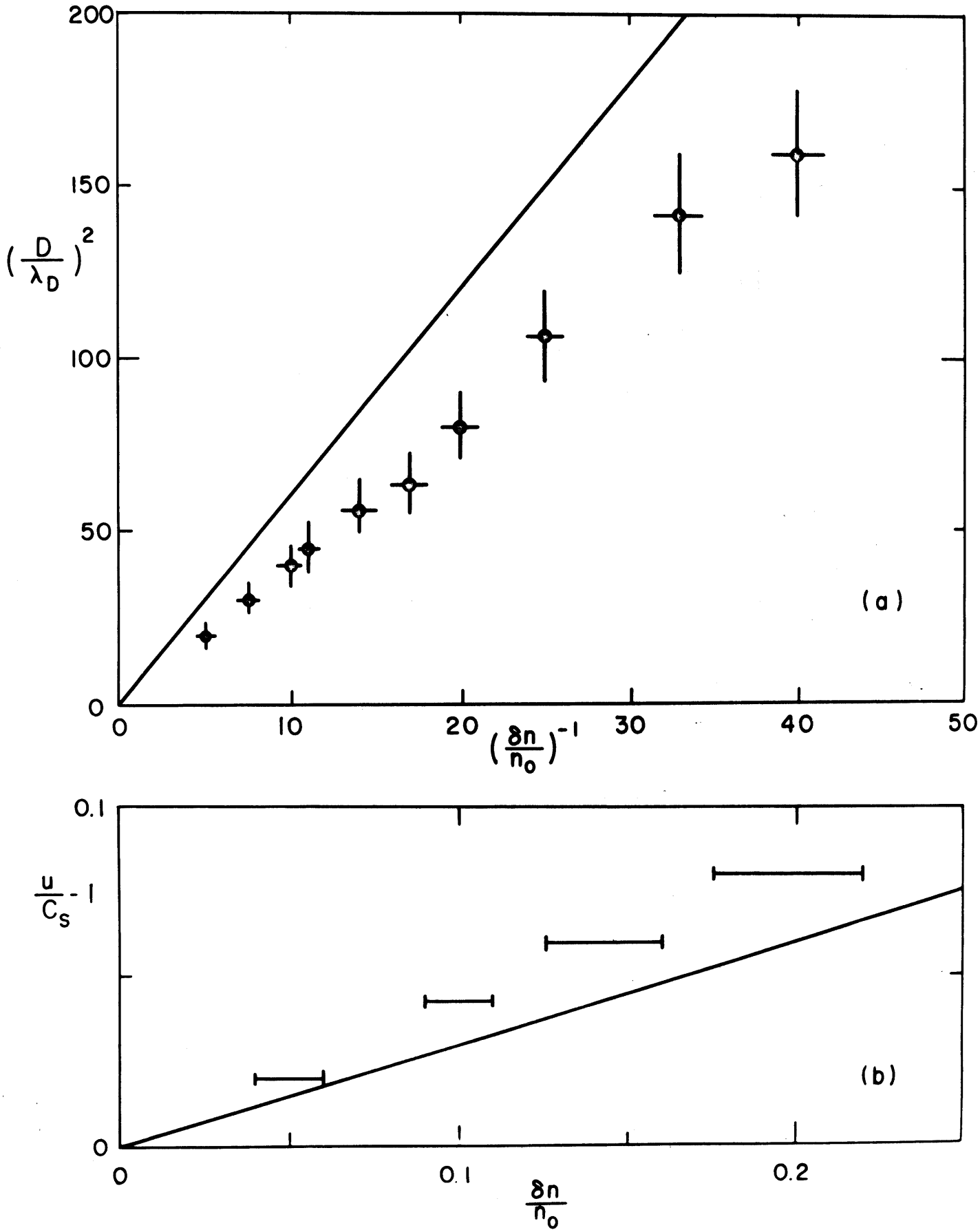
200
150
100
50
0
$(\frac{D}{\lambda_D})^2$
0
10
20
30
40
50
$(\frac{\delta n}{n_0})^{-1}$
(a)
0.1
0
$\frac{u}{C_s} - 1$
0
0.1
0.2
$\frac{\delta n}{n_0}$
(b)

FIG. 3

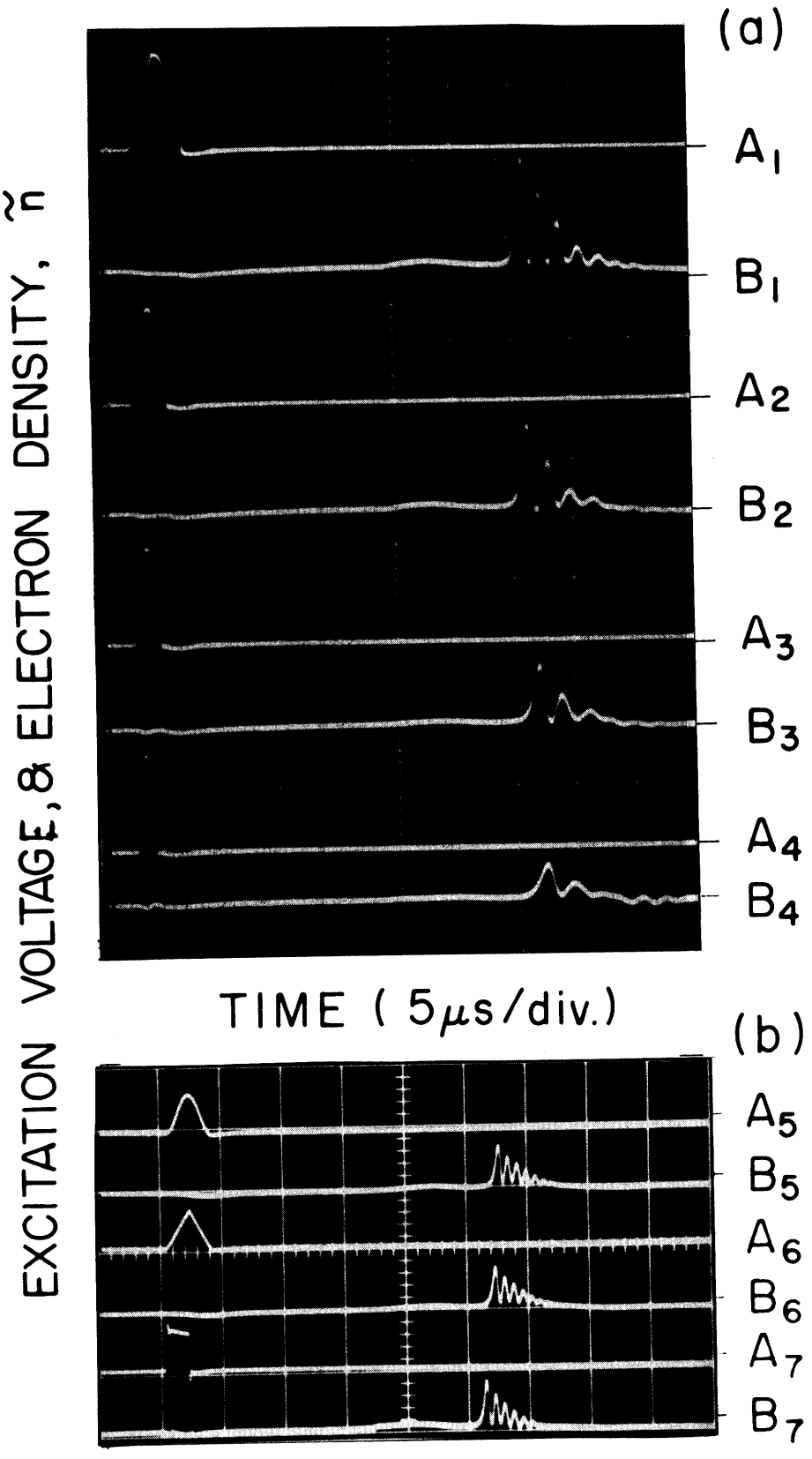
EXCITATION VOLTAGE, & ELECTRON DENSITY, ñ
(a)
A1
B1
A2
B2
A3
B3
A4
B4
TIME (5μs/div.)
(b)
A5
B5
A6
B6
A7
B7
TIME (10μs/div.)

FIG. 4

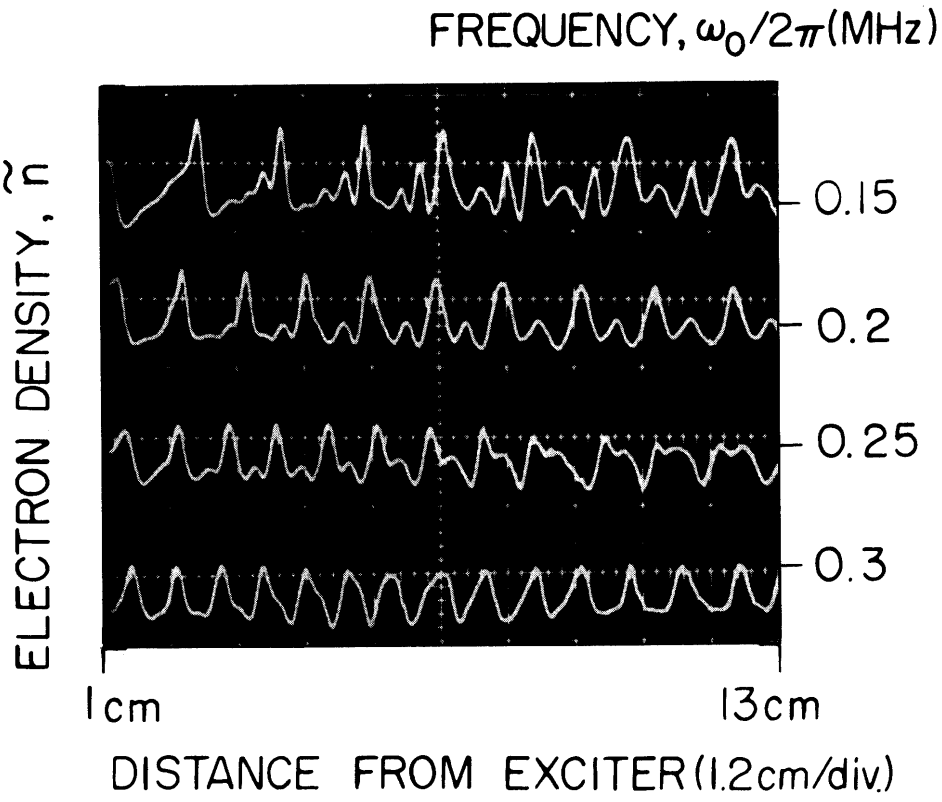
FREQUENCY, $\omega_0/2\pi$(MHz)
ELECTRON DENSITY, $\tilde{n}$
0.15
0.2
0.25
0.3
1cm
13cm
DISTANCE FROM EXCITER(1.2cm/div.)

FIG. 5

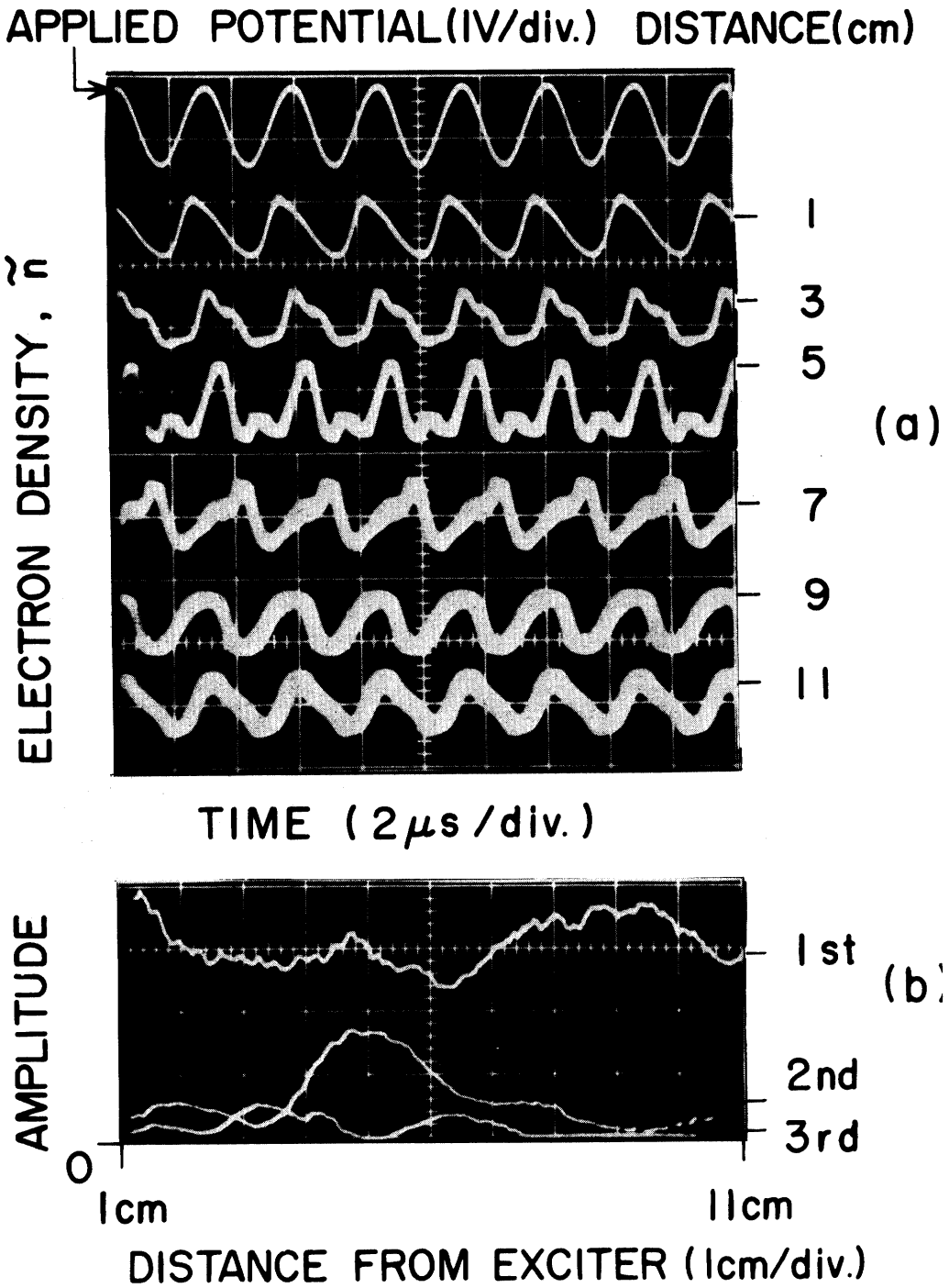
APPLIED POTENTIAL(IV/div.)
DISTANCE(cm)
ELECTRON DENSITY, ñ
1
3
5
7
9
11
(a)
TIME (2μs/div.)
AMPLITUDE
1st
2nd
3rd
(b)
0
1cm
11cm
DISTANCE FROM EXCITER (1cm/div.)

FIG. 6

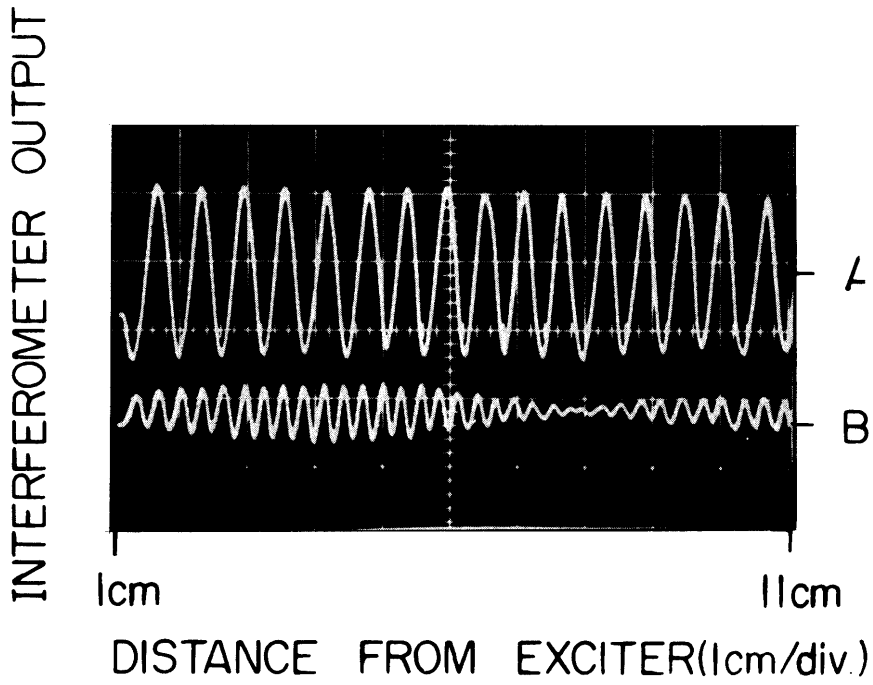
INTERFEROMETER OUTPUT
A
B
lcm
llcm
DISTANCE FROM EXCITER(lcm/div.)

FIG. 7

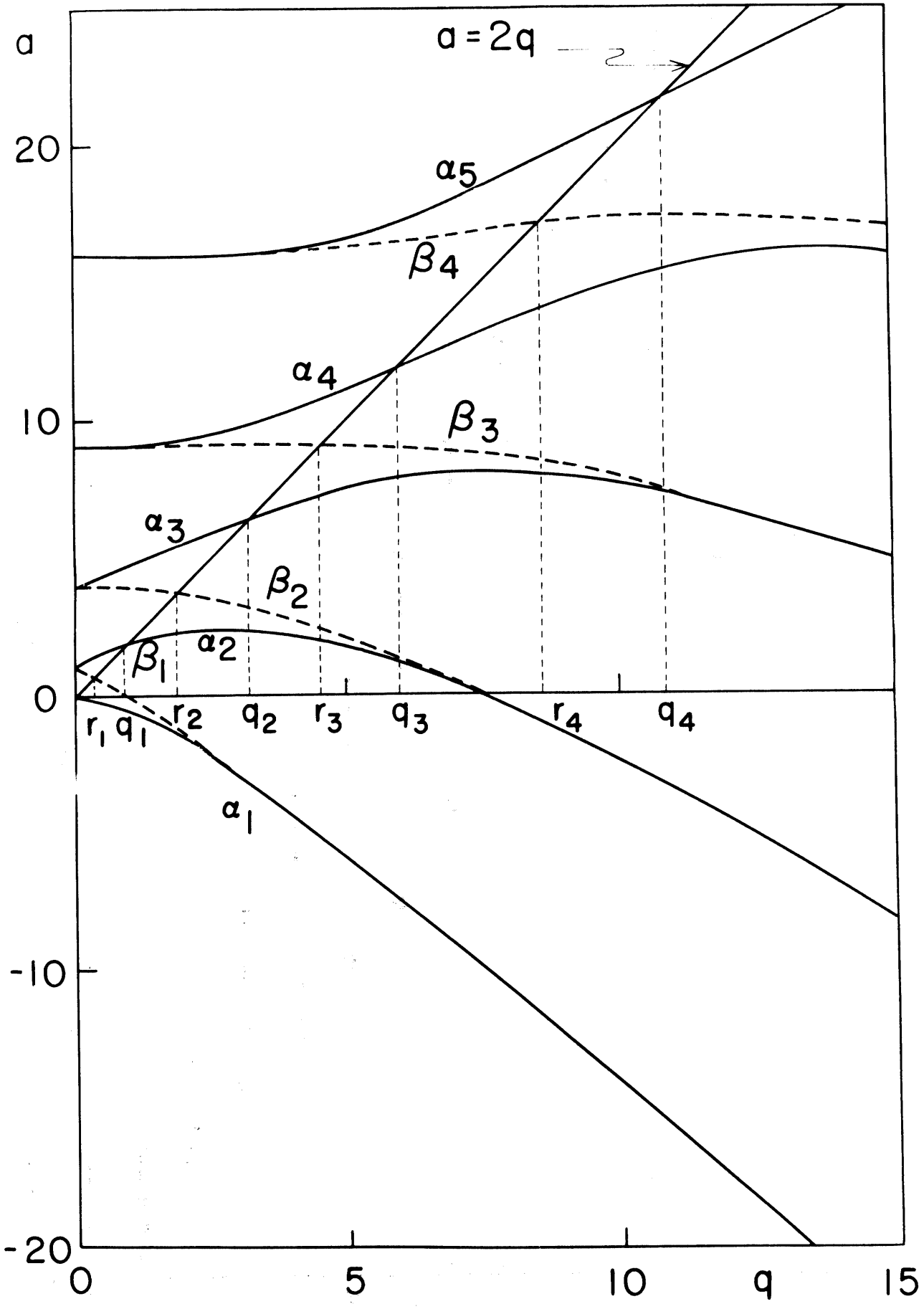
a
a = 2q
2
20
10
0
-10
-20
α_5
β_4
α_4
β_3
α_3
β_2
α_2
β_1
α_1
r_1 q_1
r_2
q_2
r_3
q_3
r_4
q_4
0
5
10
q
15

FIG. 8

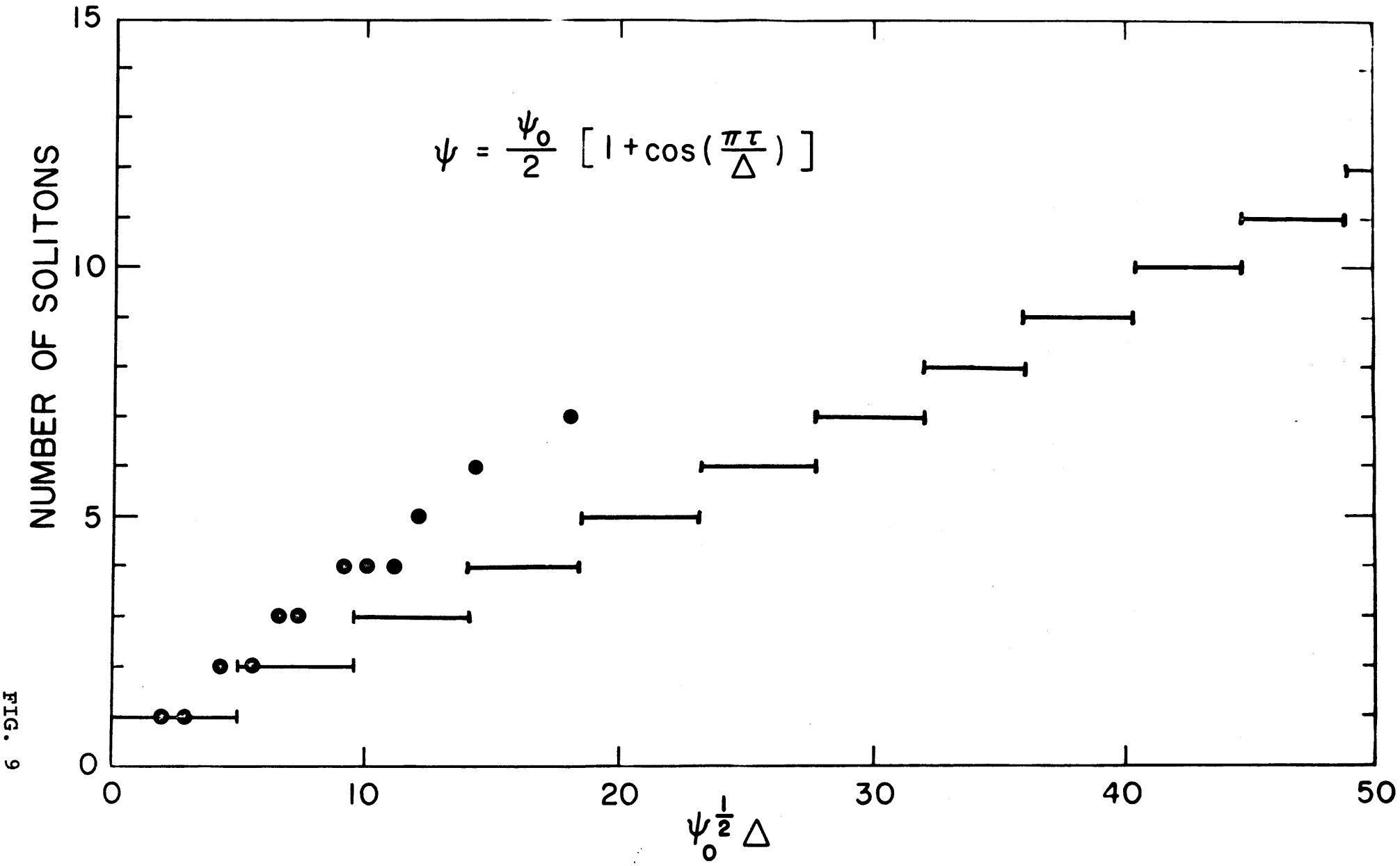
15
10
5
0
NUMBER OF SOLITONS
$\psi = \frac{\psi_0}{2}\left[1+\cos\left(\frac{\pi\tau}{\Delta}\right)\right]$
0
10
20
30
40
50
$\psi_0^{\frac{1}{2}}\Delta$

FIG. 9